PAPER

Check for updates

One-step hydrothermal preparation of Ce-doped MoO₃ nanobelts with enhanced gas sensing properties†

Zhuoqi Li, Weijie Wang, Zhicheng Zhao, Xinrong Liu and Peng Song [iD] *

Rare earth ions are considered as the ideal dopants to modify the crystal structure, electronics structure, and gas sensing performance of metal oxides semiconductors. In this paper, Ce-doped MoO_3 nanobelts were successfully synthesized *via* a one-step hydrothermal method. The morphology and microstructure were characterized by X-ray diffraction (XRD), field emission scanning electron microscopy (FESEM), energy-dispersive X-ray spectroscopy (EDS), and X-ray photoelectron spectra (XPS). FESEM images demonstrate that the as-prepared products are uniform nanobelts with length of about 20 μm and width of 100−200 nm. EDS, XRD, and XPS spectroscopy show that Ce atoms were uniformly distributed in the crystal structure of MoO_3 nanobelts. In comparison with pure samples, Ce-doped MoO_3 nanobelts exhibited superior trimethylamine (TMA) sensing properties at a lower working temperature. The effects of Ce-doping on the trimethylamine sensing performance of MoO_3 nanobelts were discussed based on the experimental results. In addition, this study provided insights and strategies for designing high performance TMA gas sensors.

Introduction

Trimethylamine (TMA) is widely used in many fields as a raw material in the chemical industry. It exists as a colorless gas with a fishy ammonia-like odour at normal temperature. Exposure to TMA gas will result in coughing, irritation of the upper respiratory system, difficulty in breathing and lung oedema.[1,2] Thus, it is very important to detect TMA accurately and quickly. Using gas sensors based on metal oxide semiconductors (MOS) is a typical method for TMA detection, such as P. M. Perillo *et al.* prepared TiO_2 membrane nanotubes to detect TMA within a concentration range of 40–400 ppm.[3] Y. H. Cho *et al.* have synthesized WO_3 hollow spheres by ultrasonic spray pyrolysis of a citric-acid-containing precursor solution, which showed high response to TMA gas.[4]

As a wide band gap semiconductor material, molybdenum trioxide (MoO_3) has corner/edge/face-sharing MoO_6 octahedron units which are capable of forming zigzag chain and unique layer/tunnel structure. It has been investigated over the past decades due to its distinctive properties of electrochromism, thermochromism and photochromism, as smart materials, catalysts and host materials for intercalation.[5–9] Furthermore, many researchers have reported the gas-sensing properties of MoO_3-based gas sensors.[10–13] For instance, using spray pyrolysis

method, R. Pandeeswari *et al.* prepared MoO_3 thin films with excellent TMA sensing performance.[14] J. H. Lee *et al.* reported MoO_3 nanoplates as TMA sensing material *via* ultrasonic spray pyrolysis technique.[15] Chu *et al.* prepared MoO_3 micro-rods and the detection limit to trimethylamine was 0.01 ppm with a sensitivity of 1.5 at 300 °C.[16] Compared with other morphologies, one-dimensional (1-D) nanostructures such as nanowires, nanobelts, and nanotubes have been demonstrated to be promising candidates for ultrasensitive sensors because of their single crystal nanostructure, high surface-to-volume ratios, specially physical and chemical properties.[17–22] S. Yang *et al.* reported ultralong MoO_3 nanobelts with length of 200 μm with excellent TMA sensing performance.[23] Our group have synthesized MoO_3 nanobelts decorated with Au nanoparticles, which exhibited highly sensitive and selective properties to trimethylamine gas.[24] Obviously, further investigation is necessary for enhancing TMA sensing performance of 1-D MoO_3 nanomaterials.

Doping, the addition of specific extrinsic element, is another effective approach to enhance the gas-sensing properties of metal oxide semiconductors.[25–31] In particularly, cerium (Ce), as a dopant to improve gas sensing performance of metal oxide, has caused widely concern and achieved certain achievements, such as Ce-doped In_2O_3 nanospheres,[32] Ce-doped SnO_2 hollow nanofibers,[33] Ce-doped ZnO thin film,[34] Ce-doped iron oxide.[35] However, to the best of our knowledge, there is a few reports on the TMA sensing characteristics of Ce-doped 1-D MoO_3 nanomaterials. Based on the above mentioned advantages of 1-D MoO_3 nanomaterials for gas sensing, as well as those associated

School of Material Science and Engineering, University of Jinan, Jinan 250022, China. E-mail: mse_songp@ujn.edu.cn; mse_songp@qq.com

with Ce doping, we synthesized pure and Ce-doped MoO_3 nanobelts by a one-step hydrothermal route. The morphology, microstructure and chemical state of as-obtained samples are characterized. In addition, the TMA sensing properties of pure and Ce-doped MoO_3 nanobelts were tested. Experimental results show that the introduction of Ce-doping is an effective way to enhance the sensing characteristic MoO_3 nanobelts toward TMA gas.

Experimental

Synthetic procedures

All the reagents we used in this experiment were of analysis grade and used without further purification. In a typical hydrothermal synthesis route, MoO_3 powders were firstly obtained by calcining $(NH_4)_6Mo_7O_{24}\cdot4H_2O$ at 500 °C for 240 min. Then, 3.6 g of as-prepared MoO_3 powders were dissolved in 27 mL of 30% aqueous H_2O_2 under vigorous stirring. Subsequently, a mixture solution of certain amount of cerium nitrate (with a mole ratio of 4%) dissolved in 13 mL concentrated nitric acid and 85 mL deionized water was added. After stirring 20 minutes at room temperature, the above solution was transferred into a Teflon-lined stainless-steel autoclave and under heat treatment at 170 °C for 48 h. After the hydrothermal reaction, the autoclave cooled naturally down to room temperature. The precipitates were collected by centrifugation, washed several times with distilled water and absolute ethanol, respectively, and dried at 60 °C for 12 h. For comparison, the pure MoO_3 nanobelts were also synthesized with the same techniques without adding cerium nitrate. The gas sensing properties were tested based on a computer-controlled WS-30A system with a static process.[24] For the target gases obtained from liquid, the concentration of target gas was calculated by the following formula,

$$C = (22.4 \times \rho \times d \times V_1)/(M \times V_2) \tag{1}$$

where C (ppm) is the target gas concentration, ρ (g mL^{-1}) is the density of the liquid, d is the purity of the liquid, V_1 (μL) is the volume of the liquid, V_2 (L) is the volume of the glass chamber, and M (g mol^{-1}) is the molecular weight of the liquid. By the formula, we can calculate the different gas concentrations.

Characterization

The crystal structure and phase composition of as-prepared samples were identified by X-ray diffraction (XRD, Bruker D8 Advance) using CuKa1 radiation ($\lambda = 0.15406$ nm) at 30 kV and 40 mA at a scanning rate of 2° at 2θ min^{-1}. The morphology and nanostructure of the products were characterized using FEI Sirion 200 field emission gun scanning electron microscope (FESEM, Hitachi S4800), and transmission electron microscopy (TEM, Hitachi H-800). The energy-dispersive X-ray spectroscopy (EDS) analysis was performed by the FESEM attachment. The X-ray photoelectron spectra (XPS) were obtained on an X-ray photoelectron spectrometer (PHI 5300) to determine the electronic structure of the surface of the Ce-doped MoO_3 nanobelts.

Results and discussion

Structure characterization

The representative morphology and microstructure of as-obtained samples are observed by FESEM. Fig. 1(a) illustrates typical FESEM image of the MoO_3 powders obtained from $(NH_4)_6Mo_7O_{24}\cdot4H_2O$ calcined at 500 °C. It can be seen that the samples are irregularly shaped particles with micron-scale size. After one-step hydrothermal treatment, the surface morphology of the pure MoO_3 samples could be clearly observed from typical FESEM image (Fig. 1(b)). From the overall morphology, it can be found that the products are uniform nanobelts with an average length of about 20 μm and width of 100–200 nm. From Fig. 1(c), the morphology of Ce-doped MoO_3 nanobelts has no obvious variation. In our experiments, the MoO_3 powders were dissolved in H_2O_2 and a transparent yellow solution was obtained after magnetic stirring. In this process, the solution-soluble precursor compound $MoO_2(OH)(OOH)$ could form easily.[36,37] In the subsequent hydrothermal growth stage, tiny MoO_3 nuclei were generated by dehydration of the dissolved yellow Mo-complex. The formation mechanism of α-MoO_3 nanobelts can be explained by the anisotropic growth of material itself. The strong preferential growth of (010) crystal plane in the [001] direction of orthorhombic α-MoO_3 forming one-dimensional structure is determined by its structural characteristics.[38–40] In the structure of α-MoO_3, distorted MoO_6 octahedra interconnect via co-edges in [001] direction (c-axis) and co-vertices in the [100] direction (a-axis). The interaction of the adjacent layers in the b-axis depends on the weak van der Waals force, whereas that replayed on the strong covalent bond in the c-axis. If the MoO_3 crystal grows in the [001] direction, the system will release more energy, in other words, the growth in the c-axis is favorable in accordance with principle of minimum energy. The energy-dispersive X-ray spectroscopy (EDS) analysis was used to further explore the existence of Ce in the doped samples. The corresponding EDS elemental mappings (Fig. 1(d–f)) indicate that the as-obtained nanobelts are composed of Mo, O, and Ce elements, and as expected, Ce is uniform distribution in the elemental mapping of Ce-doped MoO_3 nanobelts, which
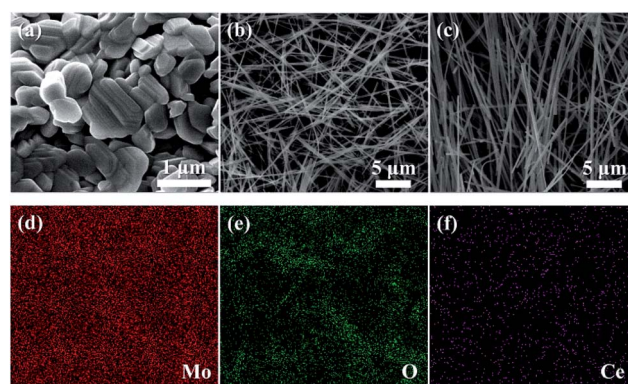

Fig. 1 (a) Typical FESEM image of MoO_3 powders; (b and c) FESEM images of pure and Ce-doped MoO_3 nanobelts, and (d–f) EDS elemental mapping of Ce-doped MoO_3 nanobelts (Mo, O, and Ce).

provide the direct evidence of the successful doping of Ce into the bulk MoO_3.

The phase purity of as-synthesized samples was characterized by XRD. As shown in Fig. 2(a), all the peaks in XRD pattern are readily agree with orthorhombic α-MoO_3 (corresponding JCPDS card No. 35-0609). For the as-prepared Ce-doped MoO_3 nanobelts, no additional diffraction peaks of cerium oxide and its related secondary or impurity phase were detected in the Fig. 2(b). The results indicated that Ce could be incorporated into the lattice of MoO_3 without affecting the orthorhombic structure of molybdenum trioxide. In order to investigate the effect of doping on the phase structures of the MoO_3 nanobelts, the (040) and (021) diffraction peaks were monitored, as shown in the inset of Fig. 2. It can be seen that the (040) and (021) diffraction peaks of Ce-doped MoO_3 shift slightly compared to the pure MoO_3. The result proved that the incorporation of Ce ions led to lattice deformation due to the difference between ionic radius of Ce [0.87 Å] and Mo [0.65 Å]. Furthermore, it can be observed that the half-width of diffraction peaks of Ce-doped MoO_3 are slightly increase compared with those of pure MoO_3. The average grain sizes are estimated using the Scherrer formula, which are about 27.64 and 23.76 nm for pure and doped samples, respectively, confirming that Ce-doping can cause the inhibition effect on crystallite size from growing up during the hydrothermal treatment, which is consistent with previous research.[41–43]

In order to investigate the chemical composition and valence state of elements, XPS analysis was characterized and the patterns are shown in Fig. 3. The XPS survey spectrum for Ce-doped MoO_3 nanobelts is presented in Fig. 3(a). The spectrum exhibits the preference of all expected core levels due to Mo 3d, O 1s, Ce 3d and C 1s. And the corresponding high resolution spectra are shown in Fig. 3(b–d). The doublets of Mo $3d_{5/2}$ and Mo $3d_{3/2}$ peaks, located at 232.3 and 235.4 eV in Fig. 3(b), correspond to Mo^{6+} in MoO_3 stoichiometric.[44] Fig. 3(c) displays the O 1s XPS spectrum of Ce-doped MoO_3 nanobelts. Two

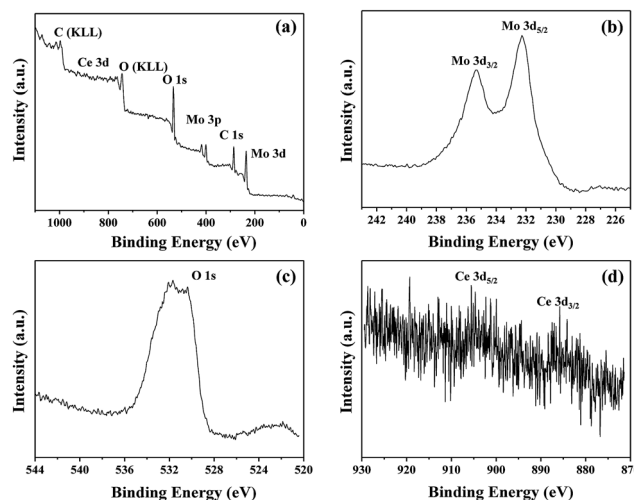

Fig. 3 XPS spectra of Ce-doped MoO_3 nanobelts. (a) Survey spectrum; (b) Mo 3d binding energy spectrum; (c) O 1s binding energy spectrum; (d) Ce 3d binding energy spectrum.

components are observed: a low binding energy (530.5 eV) is originated from the lattice oxygen in MoO_3,[45–47] and that at high binding energy (531.6 eV) is usually is assigned to the oxygen vacancies in the matrix of metal oxide,[48–50] formed due to Ce ions substitution. The results indicated that Ce-doping modified the surface state of MoO_3 nanobelts by producing oxygen vacancies, and such defects will have great influence on the gas sensing properties. Fig. 3(d) shows the Ce 3d XPS of the Ce-doped MoO_3 sample. It was reported that the Ce 3d spectra can be attributed to two sets of spin orbital multiples, $3d_{5/2}$ and $3d_{3/2}$.[51,52] As shown in Fig. 4(d), the presence of Ce^{3+} in the hybrid is confirmed by the appearance of weak signals at 885.6 and 905.1 eV.[53–55] However, the diffraction peaks of Ce^{3+} were not observed from the XRD pattern in Fig. 2, indicating that the Ce^{3+} was incorporated into the lattice of MoO_3 and had a very low content (4 mol%).
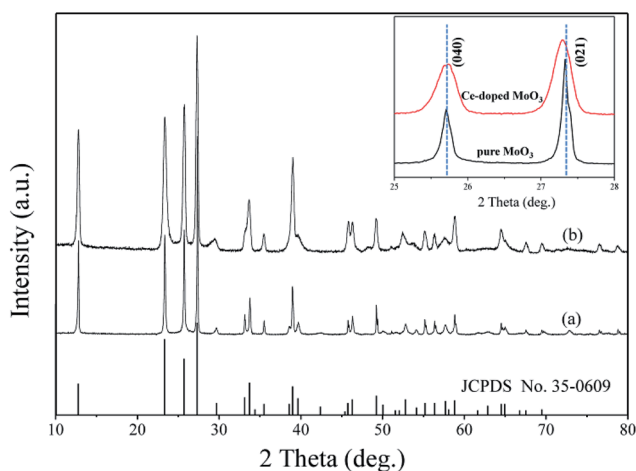

Fig. 2 XRD patterns of (a) pure and (b) Ce-doped MoO_3 nanobelts. The inset is the comparison of (040) and (021) peaks from XRD patterns.
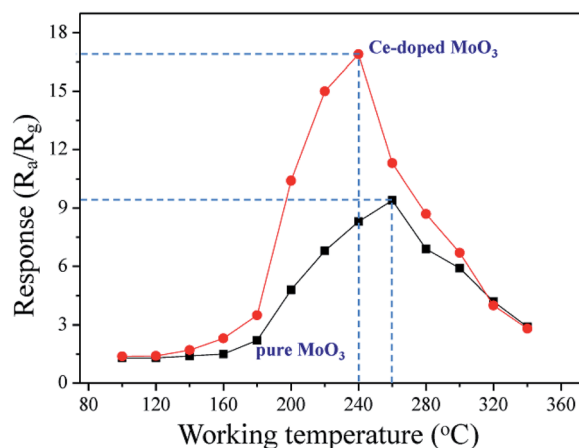

Fig. 4 Sensor response of pure and Ce-doped MoO_3 nanobelts to 50 ppm TMA gas versus working temperature.

Gas-sensing properties

As is well-known, the operating temperature is a very important parameter for gas sensors based on metal oxide. To confirm the optimum operating temperature of as-synthesized samples, we investigate the variations of the sensor response as a function of the operating temperature. As shown in Fig. 4, it can be observed that sensor based on pure MoO_3 nanobelts show relatively low response to 50 ppm TMA at the operating temperature in the range from 100 to 340 °C, with the maximum response of 4.6 at 280 °C. For compact, sensor response of Ce-doped MoO_3 nanobelts displays significant increase, reaching the maximum value of 17.4 at the operating temperature of 240 °C. Compared with pure MoO_3 nanobelts, the optimum operating temperature of the Ce-doped MoO_3 nanobelts sensor has a notable decrease. These results demonstrate that the Ce-doped MoO_3 nanobelts display about fourfold enhancement in sensor response compared to pure MoO_3, which is caused by the promotion effect of Ce-doping.

Fig. 5(a) illustrates the dynamic response and recovery curves of the sensor based on pure and Ce-doped MoO_3 nanobelts to different TMA concentrations (from 5 to 500 ppm) at 260 and 240 °C, respectively. From the curves, it is obviously found that

the response increased with an increase in TMA concentration. Specifically, the sensor based on Ce-doped MoO_3 nanobelts exhibited higher response to TMA at different concentrations compared with that of pure MoO_3 nanobelts. Previous research suggests that the concentration (C) of detected gas and the corresponding response (S) of metal oxide can be empirically represented as $S = a[C]^b + 1$. Generally for n-type semiconductor, the exponent b has an ideal value of 0.5 to 1.[56–58] As shown in Fig. 5(b), the straight lines were the calibration curves and the experimental data were fitted as:

$$y = 0.5498x + 0.3057 \qquad (2)$$

$$y = 0.3513x + 0.2710 \qquad (3)$$

where y is log(S − 1) and x is log(C). The response of both sensors have good linear relationship with the TMA concentration (5–500 ppm range) in logarithmic forms, which is in good agreement with the theory of power laws for semiconductor sensors.[59] The slope of Ce-doped MoO_3 nanobelts sensor is 0.5498, which is larger than that of pure MoO_3 nanobelts (0.3513). It indicates that the Ce-doped MoO_3 nanobelts sensor is more sensitive than the pure one, and the response of Ce-doped MoO_3 nanobelts based sensor increase faster than that of pure one accompanied with the increase of gas concentration. Gas sensing tests highlight potential application of the Ce-doped MoO_3 nanobelts in detecting TMA vapor.

Fig. 6(a) illustrates the reproducibility of the sensor based on Ce-doped MoO_3 nanobelts, revealing that the sensor maintains its initial response amplitude without obvious changes upon three successive sensing measurements to 50 ppm of TMA. In addition, within the 3 cycles, the sensor still maintains fast response and recovery state, which are demanded for practical application. The response and recovery times of Ce-doped MoO_3 nanobelts sensor to 50 ppm TMA are less than 10 and 20 s, respectively, accords with practical application of gas sensors. Moreover, the response as a function of the number of testing days was investigated and shown in Fig. 6(b). The result further indicated the splendid long-term stability of the sensor based on Ce-doped MoO_3 nanobelts.

Selectivity is an important indicator of gas sensors in practical applications. The gas responses of Ce-doped MoO_3 nanobelts towards different testing gases of 50 ppm TMA, ammonia, acetone, benzene, and ethanol are tested at 240 °C. As shown in Fig. 7, sensor response towards TMA is significantly higher than those of other gases. The selectivity of TMA is evaluated by the selectivity coefficient, which can be defined as:

$$K_{TMA} = S_{TMA}/S_{gas} \qquad (4)$$

where S_{TMA} and S_{gas} are sensor response towards TMA and any other gas. The selectivity coefficients for Ce-doped MoO_3 nanobelts based sensor were 5.2 to ammonia, 9.2 to acetone, 11.1 to benzene, and 6.0 to ethanol, indicating that Ce-doped MoO_3 nanobelts exhibit good selectivity to TMA gas.
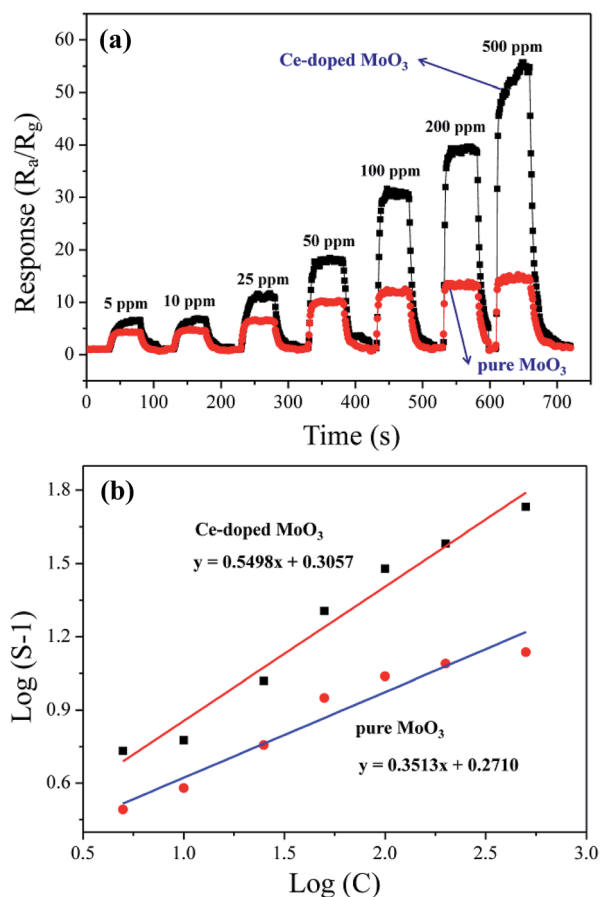

Fig. 5 (a) Relationships between sensor response of pure and Ce-doped MoO_3 nanobelts and TMA concentration and (b) the corresponding log(S − 1) vs. log(C) of the sensor based on pure and Ce-doped MoO_3 nanobelts.
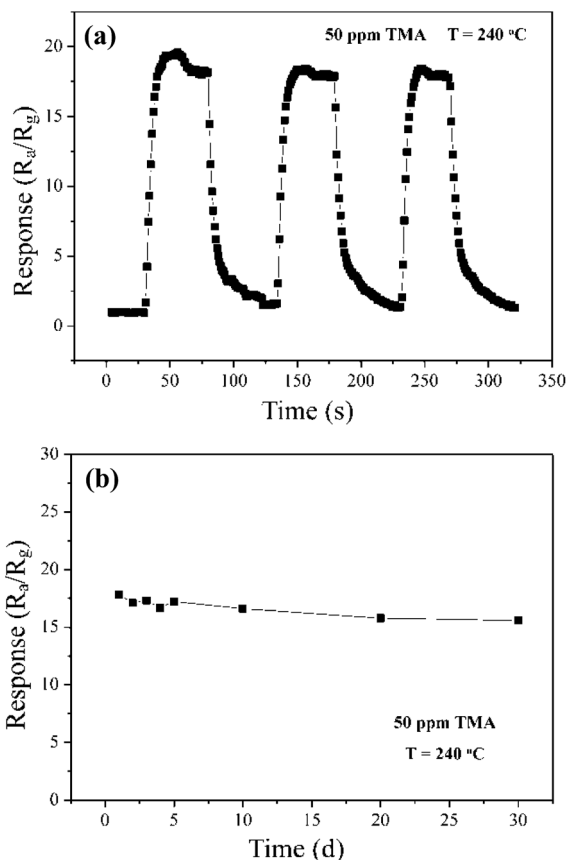
Fig. 6 (a) Three periods of response curve of Ce-doped MoO_3 nanobelts to 50 ppm TMA at 240 °C and (b) long-term stability of Ce-doped MoO_3 nanobelts sensor on successive exposure to 50 ppm TMA at 240 °C.
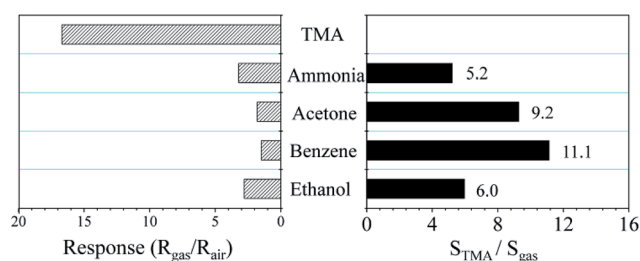

Fig. 7 Sensor response of Ce-doped MoO_3 nanobelts towards 50 ppm TMA, ammonia, acetone, benzene, and ethanol at 240 °C and the selectivity to TMA (S_{TMA} and S_{gas}, gas responses to TMA and other gases, respectively).

As generally mentioned earlier, the gas sensing mechanism of MoO_3-based sensors belongs to the surface-controlled type, which is based on the change in sensor resistance, mainly caused by the adsorption and desorption of gas molecules on the surface of MoO_3 structure.[60–62] Fig. 8 shows the adsorption and reaction model of the sensing process on the surface of pure and Ce-doped MoO_3 nanobelt. Generally, when MoO_3 nanobelts are exposed to air atmosphere, oxygen molecules are adsorbed on the surface of nanobelts, and capture electron in
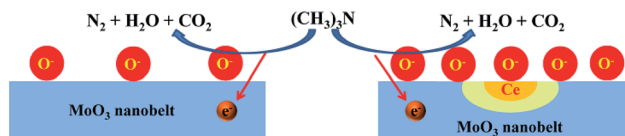

Fig. 8 Adsorption and reaction model of the sensing process on the surface of pure and Ce-doped MoO_3 nanobelt.

the surface region, forming reactive oxygen species $O_{(ads)}^-$. When injected into testing chamber, TMA gases (reducing gas) can react with reactive oxygen species O^- and release the trapped electrons back to the conduction band of MoO_3, leading to the decrease of sensor resistance, which can be written as:[63–66]

$$2(CH_3)_3N + 21O_{(ads)}^- \rightarrow N_2 + 6CO_2 + 9H_2O + 21e^- \quad (5)$$
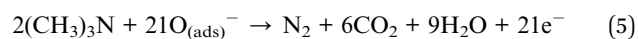
In this work, the huge improvement in gas response by Ce-doping may be due to the promotion effect of oxygen vacancy, which will be produced when Ce atom replaces Mo atom. The forming of oxygen vacancy with double positive charge can be expressed by the Kröger–Vink notation:[67]

$$CeO_2 \xrightarrow{MoO_3} Ce''_{Mo} + V_O^{\cdot\cdot} + 2O_O \quad (6)$$
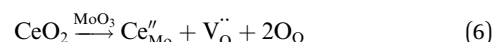
This result accords with the experiment of XPS (Fig. 3(c)). Based on the above formula, the relatively higher concentration surface oxygen vacancies can be formed due to Ce ions substitution, which is very important to the adsorption of oxygen on the surface of MoO_3 nanobelts. On exposure to air, oxygen vacancies will be reduced by the incorporation of gaseous O_2. Furthermore, as one of the most important rear-earth compounds, ceria has widely application in automobile exhaust catalysts for its stability to take and release oxygen under oxidizing and reducing conditions.[68,69] Accordingly it is also conducive to more oxygen adsorption. Thus, we believe that the Ce site works as O_2 absorbers and to some extent generate O^- adsorption sites around Ce atoms, as shown in Fig. 8. Accordingly more electrons produced by the reaction between TMA and O^- are released back to the conduction band of nanobelts, leading to higher gas response.

Conclusions

In summary, we developed a facile one-step hydrothermal route for the synthesis of pure and Ce-doped MoO_3 nanobelts. Characterizations based on XRD, EDS, and XPS displayed that Ce atoms replaced into the crystals of MoO_3 without destroying the original crystal structure. The Ce-doping is very important to the adsorption of oxygen on the surface of MoO_3 nanobelts, which is conducive to the promotion of TMA sensing properties, including lower operating temperature and enhanced gas response. Therefore, it is expected Ce-doped MoO_3 nanobelts may provide a new pathway to develop novel TMA gas sensors.

Acknowledgements

Notes and references

1 T. Hu, X. F. Chu, F. Gao, Y. P. Dong, W. Q. Sun and L. S. Bai, *J. Solid State Chem.*, 2016, **237**, 284.

2 K. Mitsubayashi, Y. Kubotera, K. Yano, Y. Hashimoto, T. Kon, S. Nakakura, Y. Nishi and H. Endo, *Sens. Actuators, B*, 2004, **103**, 463.

3 P. M. Perillo and D. F. Rodriguez, *J. Alloys Compd.*, 2016, **657**, 765.

4 Y. H. Cho, Y. C. Kang and J. H. Lee, *Sens. Actuators, B*, 2013, **176**, 971.

5 H. S. Kim, J. B. Cook, H. Lin, J. S. Ko, S. H. Tolbert, V. Ozolins and B. Dunn, *Nat. Mater.*, 2017, **16**, 454–460.

6 E. D. Hanson, L. Lajaunie, S. Q. Hao, B. D. Myers, F. Y. Shi, A. A. Murthy, C. Wolverton, R. Arenal and V. P. Dravid, *Adv. Funct. Mater.*, 2017, **27**, 1605380.

7 X. F. Yang, C. Y. Lu, J. L. Qin, R. X. Zhang, H. Tang and H. J. Song, *Mater. Lett.*, 2011, **65**, 2341.

8 X. F. Yang, H. Y. Ding, D. Zhang, X. H. Yan, C. Y. Lu, J. L. Qin, R. X. Zhang, H. Tang and H. J. Song, *Cryst. Res. Technol.*, 2011, **46**, 1195.

9 X. F. Yang, H. Tang, R. X. Zhang, H. J. Song and K. S. Cao, *Cryst. Res. Technol.*, 2011, **46**, 409.

10 S. S. Sunu, E. Prabhu, V. Jayaraman, K. I. Gnanasekar, T. K. Seshagiri and T. Gnanasekaran, *Sens. Actuators, B*, 2004, **101**, 161.

11 S. Barazzouk, R. P. Tandon and S. Hotchandani, *Sens. Actuators, B*, 2006, **119**, 691.

12 W. S. Kim, H. C. Kim and S. H. Hong, *J. Nanopart. Res.*, 2010, **12**, 1889.

13 H. H. Yan, P. Song, S. Zhang, Z. X. Yang and Q. Wang, *RSC Adv.*, 2015, **5**, 72728.

14 R. Pandeeswari and B. G. Jeyaprakash, *Biosens. Bioelectron.*, 2014, **53**, 182.

15 Y. H. Cho, Y. N. Ko, Y. C. Kang, D. Kim and J. H. Lee, *Sens. Actuators, B*, 2014, **195**, 189.

16 X. F. Chu, S. M. Liang, W. Q. Sun, W. B. Zhang, T. Y. Chen and Q. F. Zhang, *Sens. Actuators, B*, 2010, **148**, 399.

17 M. J. S. Spencer, *Prog. Mater. Sci.*, 2012, **57**, 437.

18 K. J. Choi and H. W. Jang, *Sensors*, 2010, **10**, 4083.

19 N. Lu, X. Q. Gao, C. Yang, F. Xiao, J. D. Wang and X. T. Su, *Sens. Actuators, B*, 2016, **223**, 743.

20 W. Jin, S. L. Yan, L. An, W. Chen, S. Yang, C. X. Zhao and Y. Dai, *Sens. Actuators, B*, 2015, **206**, 284.

21 G. M. Peng, S. Q. Wu, J. E. Ellis, X. Q. Xu, G. Xu, C. L. Yu and A. Star, *J. Mater. Chem. C*, 2016, **4**, 6575.

22 W. Zeng, B. Miao, T. F. Li, H. Zhang, S. Hussain, Y. Q. Li and W. J. Yu, *Thin Solid Films*, 2015, **584**, 294.

23 S. Yang, Y. L. Liu, W. Chen, W. Jin, J. Zhou, H. Zhang and G. S. Zakharova, *Sens. Actuators, B*, 2016, **226**, 478.

24 J. Zhang, P. Song, Z. Q. Li, S. Zhang, Z. X. Yang and Q. Wang, *J. Alloys Compd.*, 2016, **685**, 1024.

25 P. Li, H. Q. Fan, Y. Cai and M. M. Xu, *CrystEngComm*, 2014, **16**, 2715.

26 P. Li, H. Q. Fan, Y. Cai, M. M. Xu, C. B. Long, M. M. Li, S. H. Lei and X. W. Zou, *RSC Adv.*, 2014, **4**, 15161.

27 B. R. Koo, I. K. Park and H. J. Ahn, *J. Alloys Compd.*, 2014, **603**, 52.

28 N. D. Singh, C. Y. Yan and P. S. Lee, *Sens. Actuators, B*, 2010, **150**, 15.

29 N. Han, X. F. Wu, D. W. Zhang, G. L. Shen, H. D. Liu and Y. F. Chen, *Sens. Actuators, B*, 2011, **152**, 324.

30 S. L. Bai, C. Chen, D. F. Zhang, R. X. Luo, D. Q. Li, A. F. Chen and C. C. Liu, *Sens. Actuators, B*, 2014, **204**, 754.

31 T. Zhang, F. B. Gu, D. M. Han, Z. H. Wang and G. S. Guo, *Sens. Actuators, B*, 2013, **177**, 1180.

32 D. Han, P. Song, S. Zhang, H. H. Zhang, Q. Xu and Q. Wang, *Sens. Actuators, B*, 2015, **216**, 488.

33 P. Mohanapriya, H. Segawa, K. Watanabe, J. Watanabe, S. Samitsu, T. S. Natarajan, N. V. Jaya and N. Ohashi, *Sens. Actuators, B*, 2013, **188**, 872.

34 C. Q. Ge, C. S. Xie and S. Z. Cai, *Mater. Sci. Eng., B*, 2007, **137**, 53.

35 G. Neri, A. Bonavita, G. Rizzo, S. Galvagno, S. Capone and P. Siciliano, *Sens. Actuators, B*, 2006, **114**, 687.

36 S. Balendhran, S. Walia, H. Nili, J. Qu, S. Zhuiykou, R. B. Kaner, S. Sriram, M. Bhakaran and K. Kalantarzadeh, *Adv. Funct. Mater.*, 2013, **23**, 3952.

37 K. Segawa, K. Ooga and Y. Kurusu, *Bull. Chem. Soc. Jpn.*, 1984, **57**, 2721.

38 X. L. Li, J. F. Liu and Y. D. Li, *Appl. Phys. Lett.*, 2002, **81**, 4832.

39 L. Seguin, M. Figlarz, R. Cavagnat and J. C. Lassegues, *Spectrochim. Acta, Part A*, 1995, **51**, 1323.

40 X. W. Lou and H. C. Zeng, *Chem. Mater.*, 2002, **14**, 4781.

41 Z. Jiang, Z. Guo, B. Sun, Y. Jia, M. Q. Li and J. H. Liu, *Sens. Actuators, B*, 2010, **145**, 667.

42 C. Ge, C. Xie and S. Cai, *Mater. Sci. Eng., B*, 2007, **137**, 53.

43 P. Song, Q. Wang and Z. X. Yang, *Sens. Actuators, B*, 2012, **173**, 839.

44 S. S. Sunu, E. Prabhu, V. Jayaraman, K. I. Gnanasekar, T. K. Seshagiri and T. Gnanasekaran, *Sens. Actuators, B*, 2004, **101**, 161.

45 H. Y. Chen, H. C. Su, C. H. Chen, K. L. Liu, C. M. Tsai, S. J. Yen and T. R. Yew, *J. Mater. Chem.*, 2011, **21**, 5745.

46 O. Y. Khyzhun, T. Strunskus and Y. M. Solonin, *J. Alloys Compd.*, 2004, **366**, 54.

47 M. S. Yao, F. Ding, Y. B. Cao, P. Hu, J. M. Fan, C. Lu, F. L. Yuan, C. Y. Shi and Y. F. Chen, *Sens. Actuators, B*, 2014, **201**, 255.

48 M. Chen, X. Wang, Y. H. Yu, Z. L. Pei, X. D. Bai, C. Sun, R. F. Huang and L. S. Wen, *Appl. Surf. Sci.*, 2000, **158**, 134.

49 G. J. Yang, D. Q. Gao, Z. H. Shi, Z. H. Zhang, J. Zhang, J. L. Zhang and D. S. Xue, *J. Phys. Chem. C*, 2010, **114**, 21989.

50 Y. C. Mao, W. Li, X. F. Sun, Y. J. Ma, J. Xia, Y. F. Zhao, X. H. Lu, J. Y. Gan, Z. Q. Liu, J. Chen, P. Liu and Y. X. Tong, *CrystEngComm*, 2012, **14**, 1419.

51 T. Sukonket, A. Khan, B. Saha, H. Ibrahim, S. Tantayanon, P. Kumar and R. Idem, *Energy Fuels*, 2011, **25**, 864.

52 L. Jalowiecki-Duhamel, H. Zarrou and A. D'Huysser, *Catal. Today*, 2008, **138**, 124.

53 Z. L. Liu, B. Guo, L. Hong and H. Jiang, *J. Phys. Chem. Solids*, 2005, **66**, 161.

54 M. R. Benjaram, A. Khan, Y. Yamada, T. Kobayashi and S. Loridant, *J. Phys. Chem. B*, 2008, **107**, 5162.

55 Y. L. Kuo, C. Lee, Y. S. Chen and H. Liang, *Solid State Ionics*, 2009, **180**, 1421.

56 M. Arienzo, L. Armelao, C. M. Mari, S. Polizzi, R. Ruffo, R. Scotti and F. Morazzoni, *J. Am. Chem. Soc.*, 2011, **133**, 5296.

57 L. X. Zhang, J. H. Zhao, H. Q. Lu, L. Li, J. F. Zheng, H. Li and Z. P. Zhu, *Sens. Actuators, B*, 2012, **161**, 209.

58 X. J. Liu, Z. Chang, L. Luo, X. D. Lei, J. F. Liu and X. M. Sun, *J. Mater. Chem.*, 2012, **22**, 7232.

59 N. Yamazoe and K. Shimanoe, *Sens. Actuators, B*, 2008, **128**, 566.

60 Q. Y. Ouyang, L. Li, Q. S. Wang, Y. Zhang, T. S. Wang, F. N. Meng, Y. J. Chen and P. Gao, *Sens. Actuators, B*, 2012, **169**, 17.

61 L. N. Wang, X. Zhang, Y. Ma, M. Yang and Y. X. Qi, *Mater. Lett.*, 2016, **164**, 623.

62 A. T. Güntner, M. Righettoni and S. E. Pratsinis, *Sens. Actuators, B*, 2016, **223**, 266.

63 W. H. Zhang and W. D. Zhang, *Sens. Actuators, B*, 2008, **134**, 403.

64 R. Zhang, L. L. Wang, J. N. Deng, T. T. Zhou, Z. Lou and T. Zhang, *Sens. Actuators, B*, 2015, **220**, 1224.

65 K. M. Kim, K. I. Choi, H. M. Jeong, H. J. Kim, H. R. Kim and J. H. Lee, *Sens. Actuators, B*, 2012, **166–167**, 733.

66 C. H. Kwar, H. S. Woo and J. H. Lee, *Sens. Actuators, B*, 2014, **204**, 231.

67 F. A. Kröger and H. J. Vink, *Solid State Phys.*, 1956, **3**, 307.

68 I. Shinji, O. Hironobu, M. Takanori and K. Noriyoshi, *J. Rare Earths*, 2004, **44**, 188.

69 C. Li, K. Domen, K. I. Maruya and T. Onishi, *J. Am. Chem. Soc.*, 1989, **111**, 7683.